Silicon (2020) 12:1195–1209
https://doi.org/10.1007/s12633-019-00216-3

ORIGINAL PAPERS

Optimization of Parameters for Maximum Tensile Strength of Friction Stir Welded AA6082/Si_3N_4 and AA6082/SiC Composite Joints

Rajesh Kumar Bhushan [1] · Deepak Sharma [2]

Received: 31 March 2019 / Accepted: 13 June 2019 / Published online: 8 July 2019

Abstract
Weldability, microstructure evolution and tensile strength of an aluminium alloy (AA6082) and of two category of composites with AA6082 matrix reinforced with Si_3N_4 and SiC particles during friction stir welding (FSW) were investigated. 5, 10 and 15 weight percentage of reinforced particle were used in each category. FSW was carried out as per the parameters selected by Taguchi L-9 orthogonal Array. Microstructure of nugget region was investigated by scanning electron microscopy (SEM) and EDS analysis. Effect of tool rotational speed, welding speed and tool tilt angle on tensile strength was also investigated. The optimum parameters to get maximum ultimate tensile strength (UTS) for AA6082/SiC and AA6082/ Si_3N_4 composites were found out. On one hand, SiC particles are fractured thus fined due to intensive stirring action during FSW. On the other hand, the plastic flowing of material in the weld is benefit to eliminate microporocities existed in original base material. The highest tensile strength of 193 MPa was obtained for AA6082/15 wt% Si_3N_4 composite, at tool rotation speed of 1950 rpm at fixed welding speed of 40 mm/min and fixed tool tilt angle of 2°. Hard Si_3N_4 particles transfer their strength to the AA6082 matrix by their strengthening mechanism. This happens because of load transfer from Si_3N_4 particles to AA6082 matrix.

Keywords Tensile strength · Taguchi L-9 orthogonal Array · AA6082/Si_3N_4 · AA6082/SiC welding speed · Rotation speed · Tool tilt angle

1 Introduction

Automotive, aerospace, shipbuilding, and railway industries develop products of various shape. High strength to weight ratio materials are needed to reduce overall weight of the product without compromising the quality. This is necessary to further improve the performance of various products. Limitations of conventional welding methods are porosity, more residual stresses, separation, lack of fusion, contraction during solidification. These methods also have high solubility of hydrogen and other gases. Strength of the weld is reduced because of these limitations. FSW is a solid state non-conventional joining technique. FSW overcomes the above limitations. Quality and strength of FSW can be assessed by tensile strength. This is because the tensile failure takes place along the weakest path.

Not much work has been reported about, FSW of the metal matrix composites (MMCs). Research into FSW of MMCs needs because of diversified industrial requirements. To obtain high quality FSW joints of Al based MMCs, welding should be carried out under appropriate parameters [1, 2]. Microstructural aspects of the dissimilar joints were investigated by varying the material on the advancing side (AS) and the number of welding passes [3, 4]. Researcher studied microstructure and mechanical properties of Al2009-SiC MMCs and 2024 alloy. Microstructural evolution and the material flow during FSW are typical issues. These are mostly dependent on the tool geometry and the process parameters. Tensile strength up to 85% of the 2024 Al alloy was achieved in the FSW joints of Al2009-SiC MMCs and 2024 alloy. Hence, research is further needed in FSW of MMCs to obtain higher values of tensile strength [5]. Rice husks (RH) contain organic substances and 20% of inorganic material. Some attempts

✉ Rajesh Kumar Bhushan
rkbsmvdu@gmail.com

Deepak Sharma
erdeepak786@gmail.com

[1] Guru Ghasidas Vishwavidyalaya (A Central University), Bilaspur, Chhatisgarh, India

[2] Shri Mata Vaishno Devi University, Katra, Jammu and Kashmir, India

have been made by reseachers to produce advanced materials – including SiO_2, SiC, Si_3N_4, elemental Si, Mg_2Si and more recently active carbon, using RH [6]. Soltani, et al. [7] carried out critical review on the processing and application of rice husks for the production of various silicon-based materials and of active carbon. They addressed the different processing methods, activating conditions and activated carbon consolidation mechanisms. Rice husk ash (RHA) as an important oxygen source was incorporated into SiC porous preforms. Effect of rice-husk ash on properties of laminated and functionally graded Al/SiC composites by one-step pressureless infiltration was analysed [8]. Wettability behavior of B_4C substrate as well as B_4C /crystalline rice husk ash and B_4C /amorphous rice husk ash substrates with two aluminum alloys were studied. Boron carbide substrates after addition of amorphous or crystalline rice husk ash display good wettability with molten aluminium alloys [9].

Authors used Al-Mg-Si alloy as matrix. 10 weight percentage of Al_2O_3 particulates along with 0, 2, 3, and 4 weight percentage of RHA were added in the matrix. MMCs were fabricated by two-step stir casting method. 3.56% reduction in tensile strength was observed for 8% and 13% RHA composites. 7.7% lower specific strength was obtained for 3 weight percentage of and 4 weight percentage of RHA composites [10]. Soltani, et al. [11] carried out three-step study to enhance wettability of RHA by Al-Mg-Si alloys. Si_3N_4 was coated on RHA by hybrid CVI system, using solid precursor of Na_2SiF_6. Optimum processing parameters to maximize the amount of deposited Si_3N_4 were defined. Contact angle decreased from 72 to 35 degree due to coating of RHA with Si_3N_4. Bahrami, et al. [12] carried out an investigation on the wetting behavior of three substrate types (SiC, SiO_2-derived RHA and SiC/SiO_2 derived RHA) by two Al–Si–Mg alloys in nitrogen atmosphere, using the sessile drop method. Results indicated that in the case of silica substrates, mostly there is a transition from non-wetting contact angles (obtuse values) to wetting contact angles (acute values) and that the lowest values of θ are achieved with the high Mg alloy in contact with amorphous SiO_2. Authors investigated effect of SiC particles on mechanical properties. Increase in the elastic modulus of Al-SiCp composites with increase in the weight percentage of SiC particles was observed. Elastic modulus of composites with 10 wt.% SiCp was found to be 8.6% higher than that of the AA 5083 Al alloy. Tensile strength increased with increase in weight percentage of SiC particles [13]. FSW of 16 mm thick AA 6061-T6 plates was carried out. This was done at tool rotational speeds of 500, 700, and 900 rpm. Welding speed of 120 mm/min was maintained. It was found that the longitudinal residual stress distribution is an M shaped distribution in the transverse direction; in weld region. Value of tensile longitudinal stress in the advancing side was found to be more than that in the retreating side [14].

Above literature review show that little work has been reported about tensile strength of FSW joints of MMCs plates. Novelty of work is that, in the published literature little work has been reported about the optimization of process parameter to obtain maximum tensile strength and comparison of tensile strength of AA6082/SiC and AA6082/Si_3N_4 composites. Outcome of this research work would be useful for joining the components made of composites, by FSW. These parts would be used in aircraft, satellite, automobiles and ships. Objectives of this investigation are the study of weldability, microstructure evolution and tensile strength of AA6082/SiC and AA6082/Si_3N_4 composites and focus is put on the optimization of welding parameters to get maximum UTS for AA6082/SiC and AA6082/ Si_3N_4 composites.

2 Experimental Works

2.1 Base Material

Commercially available AA6082-T6 is used as base material in this research work. Chemical composition as well as mechanical properties of the matrix alloy are given in Tables 1 and 2, respectively.

2.2 Fabrication

2.2.1 Fabrication of AA6082/Si_3N_4 Composites

AA6082/ Si_3N_4 composites was fabricated using AA6082-T6. Reinforcing particles were Si_3N_4. 900 g of AA6082 was liquefied at 850 °C in graphite crucible. Rotation of liquefied mixture was carried out for 12 min to attain homogeneous distribution of Si_3N_4 in the AA6082 melt. Stirring was carried out at 230 rpm, to form a fine vortex. A mechanical stirrer was used for this. Si_3N_4 ceramic powder was preheated in oven at 530 °C. This was done to oxidize the surface of Si_3N_4 particles. Warmed Si_3N_4 powder was fed at a continuously, in the AA6082 melt. Temperature of molten mixture was gradually increased to 940 °C. During stirring process argon gas was supplied into the liquefied mix. This was done to maintain an inert atmosphere. After completing the stirring of AA6082/ Si_3N_4 molten mixture, it was poured into a preheated permanent mould. Argon gas continued to supply till the complete molten mixture was poured into the preheated (280 °C) permanent mould. Fabricated AA6082/ Si_3N_4 composites were permitted to solidify in open atmosphere. They were removed

Table 1 Chemical composition of AA6082-T6 in wt%

Element	Al	Si	Mg	Mn	Fe	Cu	Cr	Zn	Ti	Vn
(wt%)	97.3	.92	0.68	0.57	0.23	0.07	0.035	0.098	0.019	0.01

Table 2 Mechanical properties of AA6082-T6

Tensile strength (MPa)	Proof stress (0.2% MPa)	Density (g/cm^3)	Vickers hardness (HV)	% Elongation (min %)
320	310	267	100	9

from the mould after whole solidification. Composites having different weight percent (5, 10 and 15%) of Si_3N_4 particles were fabricated by the same apporach.

2.2.2 Fabrication of AA6082/SiC Composites

Samples were fabricated by stir-casting process. AA6082 was placed in a crucible made of graphite. Then crucible was placed inside an electrical resistance furnace. Temperature was gradually increased to 900 °C. Four blade stirrer was used to stir the melt. Enough stirring was done for homogenous SiC particle distribution throughout the AA6082 melt. 5% by weight SiC particles were heated at 800 °C for 120 min before putting them in crucible. Heated SiC particles were placed in the AA6082 melt. Mixture was continuously stirred. Mixture of AA6082 and SiC was heated at 900 °C for 2 h. Mixture was stirred twice for 20 min each at interval of 1 h. This was done to attain uniform distribution of particles. Nitrogen gas was fed into the mixture during rotation of mixture. This was done to eliminate the formation of oxide layer on the top surface of mixture melt. After mixing liquid mixture was poured in pre heated permanent mould. Same procedure was adopted to prepare, AA6082/SiC/10 wt% and AA6082/SiC/15 wt% composites. Specimens were cut from the ingots. These specimens were smoothened by emery paper. Further specimens were polished with 3-μm sized diamond paste for metallographic examinations. Plates were prepared from AA6082, AA6082/SiC and AA6082/Si_3N_4 composites for FSW. Samples were collected from the nugget area after FSW of AA6082/SiC/5_P, AA6082/SiC/10_P, AA6082/SiC/15_P and AA6082/Si_3N_4/5_P, AA6082/Si_3N_4/10_P, AA6082/Si_3N_4/15_P for tensile tests.

2.3 Characterization Techniques

Following techniques were used for characterization of AA6082, AA6082/SiC/5_P, AA6082/SiC/10_P, AA6082/SiC/15_P and AA6082/Si_3N_4/5_P, AA6082/Si_3N_4/10_P, AA6082/Si_3N_4/15_P composites.

2.3.1 Scanning Electron Microscopy

Specimens were cut from the ingots. These specimens were prepared for metallographic examinations using 220–320–500–1000 mesh emery papers, followed by polishing with 2-μm sized diamond paste. Scanning electron microscope (QUANTA 200FEG (FEI, Eindhoven, the Netherlands) equipped with energy dispersive X-ray analyses (EDAX) was used to study the composite structure.

2.3.2 Energy Dispersive X-Ray Analyses (EDAX)

The samples were examined using scanning electron microscopy (SEM) QUANTA 200FEG, FEI Netherland equipped with energy dispersive X-ray analyses (EDAX). This curve shows various peaks and analysis gives weight and atomic weight percentage of different elements in the samples under examination.

2.3.3 Tensile Testing Machine

Tensile testing of friction stir welded joints is necessary to know how much tensile load the joint can sustain when subjected to industrial application. FIE make UNITEK 94100 model UTM was used to find out tensile strength. Sketch map of tensile test specimen as per ASTM: E8/E8 M-13a standard is shown in Fig. 1.

2.4 FSW Parameters

FSW parameters in this research work are tool rotation speed (rpm), welding speed (mm/min) and tool tilt angle (degree). Taguchi's L9 array has been used to decide FSW parameters. Three levels of all the three parameters are shown in Table 3. Minitab software has been used for calculation and analysis.

Bilici, [15] used the L_9 orthogonal array of Taguchi, to design and optimize the experiments. Composite plates of size 100 × 50 × 6 mm were mounted on the FSW fixture on the vertical milling machine table. Tool was then plunged into the work pieces and sufficient dwell time was given to allow the tool to generate the desired heat for welding. Tool was then fed through the weld line at specified welding speed and the FSW of the composite plates was accomplished. After welding, the specimens were cut out of the weld samples.

3 Results

3.1 Tensile Test

Tensile strength of AA6082 alloy and fabricated AA6082/SiC and AA6082/Si_3N_4 composites are shown in Table 4. Results show that the tensile strength of AA6082 alloy increases with addition of SiC/5_P, SiC/10_P and /SiC/15_P into AA6082 alloy.

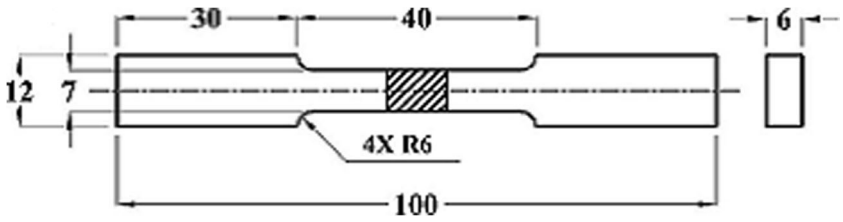

Fig. 1 Sketch map of tensile test specimen

Also there is gradual increase in tensile strength of AA6082 alloy due to mixing of $Si_3N_4/5_P$, $Si_3N_4/10_P$ and $Si_3N_4/15_P$ particles in to it.

3.2 Tensile Test of Friction Stir Welded AA6082 Alloy and Fabricated AA6082/SiC and AA6082/Si_3N_4 Composites

Tensile test results of friction stir welded AA6082, AA6082/SiC and AA6082/Si_3N_4 composites are shown in Table 5.

3.3 Variation in Ultimate Tensile Strength of AA6082 and AA6082/SiC Composites

Change in UTS of AA6082 and AA6082/SiC composites is shown in Fig. 2. There is gradual increase in tensile strength of AA6082 due to addition of 5, 10, 15 vol% SiC particles.

3.3.1 Change in Microstructure of Weld Nugget of AA6082/SiC Composite

Figure 3 Shows SEM image of as casted AA6082. Figure 4 shows the SEM micrographs of AA6082 reinforced with 5 wt% SiC particles. Micrographs clearly indicate the presence of SiC particles in the AA6082 matrix. Distribution of SiC particles is observed to be mostly homogeneous. There are no clusters or accumulation of SiC particles. Figure 5 shows SEM micrographs of AA6082 reinforced with 10 wt% SiC particles. No separation of SiC particles is seen along the grain boundaries. Near the grain boundaries some SiC particles are seen. Figure 6 presents the SEM micrographs of AA6082/SiC/15_P composite. Interface between the AA6082 matrix and the SiC particles can be seen in these figures. Every SiC particle is attached within the AA6082 matrix

3.3.2 Phase Formation by EDX Analysis of AA6082/SiC Composite

EDX patterns of the 6082 Al alloy reinforced with 5 wt.%, 10 wt% and 15 wt% SiC particles are shown in Figs. 7, 8 and 9. The EDX pattern confirmed the presence of aluminum matrix and SiC particulate in the composite.

Element analysis of Fig. 7 shows that main element at nugget zone are; Al 73.06%, Si 3.88%. Main element at nugget zone as per Fig. 8 are; Al 77.98%, Si 4.89%. Element analysis of Fig. 9 shows that main element at nugget zone are; Al 48.06%, Si 13.11%.

3.4 Variation in Ultimate Tensile Strength of AA6082 and AA6082/Si_3N_4Composites

Change in UTS of AA6082 and AA6082/Si_3N_4 composite is shown in Fig. 10. Figure 10 shows that there is gradual increase in UTS of AA6082 due to addition of 5, 10, 15 vol% Si_3N_4 particles.

3.4.1 Change in Microstructure of Weld Nugget of AA6082/Si_3N_4 Composite

Comparatively good dispersion of reinforced particles is seen in Figs. 11 and 12. In Fig. 13 formation of dendritic region is mainly due to cooling of fabricated AA6082/Si_3N_4 composites while solidification. Thermal conductivity of Si_3N_4 particles is less in comparison to AA6082. Because of this, the temperature

Table 3 Taguchi's L9 array of FSW parameters

Experiment No.	Tool rotation speed (rpm)	Welding speed (mm/min)	Tool tilt angle (degree)
1	1540	30	1
2	1540	40	2
3	1540	50	3
4	1950	30	3
5	1950	40	2
6	1950	50	1
7	2300	30	1
8	2300	40	3
9	2300	50	2

Table 4 Tensile test results of unwelded AA6082 and fabricated AMCs

Composition	As casted AA6082	AA6082/ $SiC/5_P$	AA6082/ $SiC/10_P$	AA6082/ $SiC/15_P$	AA6082/ $Si_3N_4/5_P$	AA6082/ $Si_3N_4/10_P$	AA6082/ $Si_3N_4/15_P$
Average ultimate tensile strength (MPa)	139.63	146.23	161.77	176.36	169.66	180.91	193.15

of Si_3N_4 particles is high as compared to molten AA6082. As a result, hot Si_3N_4 particulates take extra time to cool when solidifying. Creation of dendritic area is because of cooling of fabricated AA6082/Si_3N_4 composites at the time solidification.

3.4.2 Phase Formation by EDX Analysis AA6082/ Si_3N_4 Composite

EDX patterns of the AA6082/Si_3N_4 composites provides the details about the different elements existing in the fabricated composites. EDX pattern analysis shown in Figs. 14, 15 and 16 confirms the presence of Si_3N_4 particulates within the aluminium matrix. The peak of Si and N is clearly visible in the EDX pattern.

Element analysis of Fig. 14 shows that main element at nugget zone are; Al 79.74%, Si 4.49%, N 0.29%. Main element at nugget zone as per Fig. 15 are; Al 79.53%, Si 5.66% N 0.13%. Element analysis of Fig. 16 shows that main element at nugget zone are; Al 77.91%, Si 5.6% N 1.57%. The EDX results reveal that main elements present are Al (largest peak) and Si (second largest peak) and N (lower peak).

3.5 Variation in Ultimate Tensile Strength of Weld Nugget of AA6082/ SiC Composite with Tool Rotation Speed

Figure 17 show the change of UTS with increase of tool rotation speed, at fixed welding Speed of 40 mm/min and fixed tool angle of 2°. UTS of AA6082 increases from 130 to 132 MPa with increase of tool rotation speed from 1550 to 1950 rpm. UTS of AA6082/$SiC/5_P$ composites increases from 117 to 120 MPa with increase of tool rotation speed from 1550 to 1950 rpm. UTS then starts decreasing with increase of tool rotation speed from 1950 to 2300 rpm, both for AA6082 and AA6082/SiC/5_P composite. UTS of AA6082/$SiC/10_P$ composites increases from 128 to 137 MPa with increase of tool rotation speed from 1550 to 1950 rpm. UTS then starts decreasing from 137 to 129 MPa with increase of tool rotation speed from 1950 to 2300 rpm. While a different trend is observed for AA6082/$SiC/15_P$ composite. UTS of AA6082/$SiC/15_P$ composites continuously increases from 125 to 148 MPa with increase of tool rotation speed from 1550 to 2300 rpm. When the tool rotation speed varies from 1500 to 1950 rpm, the tensile strength of AA6082 varies from 130 to 132 MPa. Parent metal exhibit higher tensile strength of 134.53 MPa. Of the welded joints, the joint of AA6082/$SiC/15_P$ and AA6082/$SiC/15_P$ composites fabricated using tool rotation speed of 1950 rpm yielded higher tensile strength of 136 MPa which is 11.67% lower than the parent metal strength.

Variations of UTS with tool rotational speed are shown in Fig. 17. Increasing trend in weld joint strength is observed due to increase in the rotational speed (up to 1950 rpm). Decreasing trend in weld joint strength is seen with further

Table 5 Tensile test results of friction stir welded AA6082 alloy, AA6082/SiC composites and AA6082/Si_3N_4 composites

Sample No. according to Taguchi L9 array	Ultimate tensile strength (MPa)						
	As casted AA6082	AA6082/ $SiC/5_P$	AA6082/ $SiC/10_P$	AA6082/ $SiC/15_P$	AA6082/ $Si_3N_4/5_P$	AA6082 /Si_3N_4/ 10_P	AA6082 /Si_3N_4/ 15_P
1	131.65	122.93	132.68	127.21	134.31	149.89	133.93
2	129.23	116.08	126.83	127.44	133.98	136.11	142.71
3	129.86	113.56	127.39	119.29	123.42	137.03	136.34
4	134.53	123.24	139.47	141.71	142.27	159.72	168.79
5	132.66	120.76	138.64	136.68	138.51	158.96	156.33
6	130.94	118.73	132.53	129.42	133.53	158.13	153.09
7	129.47	113.23	131.88	153.95	145.67	156.86	171.19
8	128.33	114.69	128.26	146.17	132.73	158.2	163.7
9	122.87	109.44	124.72	141.04	113.19	139.57	149.42
Mean	129.94	116.96	131.37	135.87	133.06	150.49	152.83

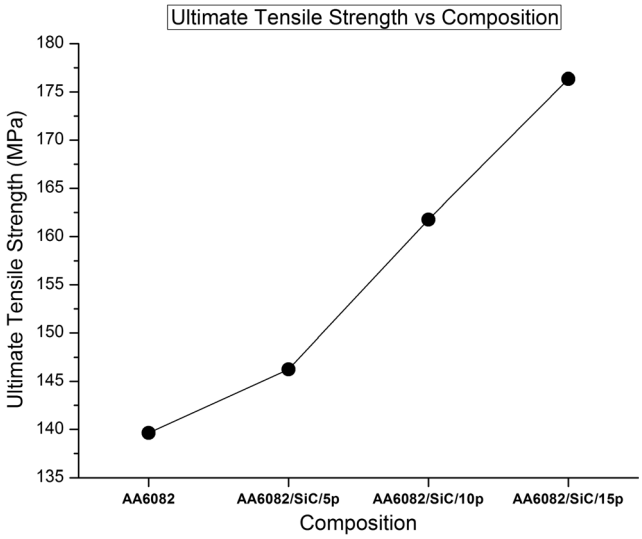

Fig. 2 Change in UTS of AA6082 and AA6082/SiC Composites

increase in rotational speed (>1950 rpm). More plasticized weld material was generated at higher tool rotational speed. This is because of high frictional heat. Which resulted in thinning of welded area. Weld strength decreased at high rotational speed, due to local thinning.

Three joints were obtained at different rotational speed. Lower tensile strength was observed for joints fabricated at the rotational speed of 1500 rpm and 2300 rpm as compared to the joints fabricated at a rotational speed of 1950 rpm. Tensile properties of the joints fabricated at a rotational speed of 1950 rpm are superior as compared to other joints.The maximum tensile strength at 1950 rpm can be ascribed to minimum hardness variation. Strength of FSW joint will be maximum, when the tool rotational speed provides sufficient stirring of plasticized material and good amalgamation of the same at the retreading side. When tool rotational speed increases beyond 1950 rpm, the stirring becomes counterproductive. This influence the rate of material transfer from advancing side to retreading side. As a result tensile strength reduces.

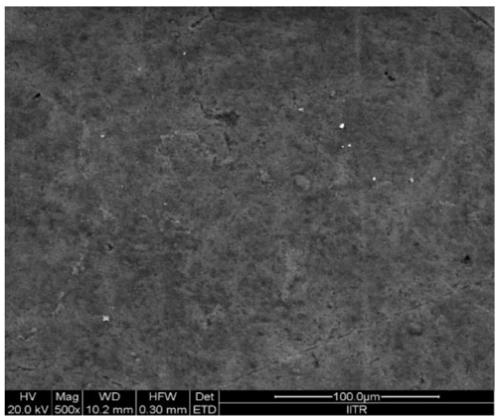

Fig. 3 SEM image of as casted AA6082

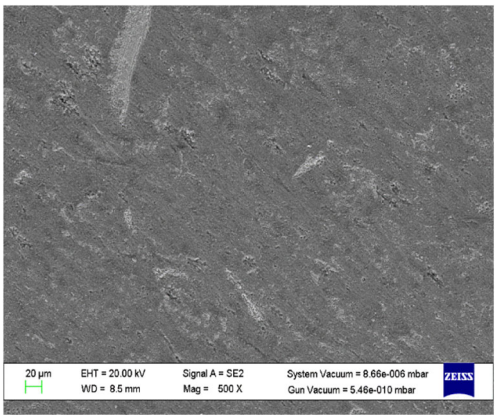

Fig. 4 SEM image of AA6082/SiC/5_P

3.6 Variation in Ultimate Tensile Strength of Weld Nugget of AA6082/ Si_3N_4 Composite with Tool Rotation Speed

Figure 18 show the change of UTS with increase of tool rotation speed, at fixed welding Speed of 40 mm/min and fixed tool tilt angle of 2°. UTS of AA6082 increases from 130 to 132 MPa with increase of tool rotation speed from 1550 to 1950 rpm. UTS of AA6082/$Si_3N_4/5_P$ composites increases from 130 to 138 MPa with increase of tool rotation speed from 1550 to 1950 rpm. UTS then starts decreasing with increase of tool rotation speed from 1950 to 2300 rpm, both for AA6082 and AA6082/$Si_3N_4/5_P$ composite. UTS of AA6082/$Si_3N_4/10_P$ and AA6082/$Si_3N_4/15_P$ composites increases from 140 to 160 MPa with increase of tool rotation speed from 1550 to 1950 rpm.

UTS then starts decreasing from 160 to 152 MPa with increase of tool rotation speed from 1950 to 2300 rpm, for AA6082/$Si_3N_4/10_P$. But for AA6082/$Si_3N_4/15_P$ composite it increases from 160 to 162 MPa. AA6082/$Si_3N_4/5_P$ composite FSW joint fabricated using 1950 rpm yielded tensile strength of 138 MPa which is 6% higher than the parent metal. When the tool rotation speed increases to 2300 rpm, the tensile strength dramatically decreases to

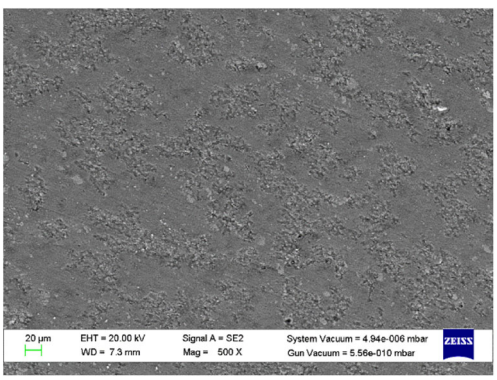

Fig. 5 SEM image of as casted AA6082/SiC/10_P

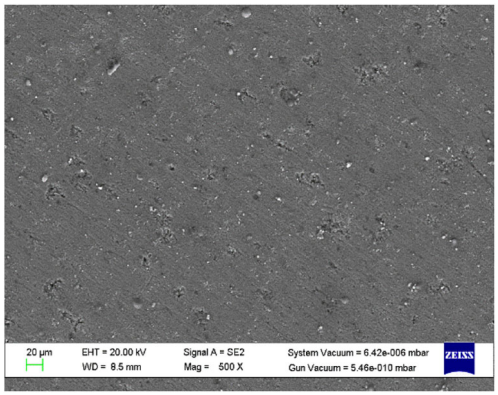

Fig. 6 SEM image of AA6082/SiC/15_P

a relatively low value, except of AA6082/ $Si_3N_4/15_P$ composites owing to the formation of the cavity defect on the AS and adjacent to the top surface.

3.7 Variation in Ultimate Tensile Strength of Weld Nugget of AA6082/ SiC Composite with Welding Speed

Figure 19 show the change of UTS with increase of welding Speed, at fixed tool rotation speed of 1950 rpm and fixed tool tilt angle of 2°. UTS of AA6082 decrease from 133 to 130 MPa with increase welding speed from 30 to 50 mm/min. UTS of AA6082/SiC/5_P composites decreases from 120 to 112 MPa with increase welding speed from 30 to 50 mm/min. UTS of AA6082/SiC/10_P composites decreases from 135 to 130 MPa with increase welding speed from 30 to 50 mm/min. UTS of AA6082/SiC/15_P composites decreasesfrom142 to 132 MPa with increase welding speedfrom30 to 50 mm/min.

3.8 Variation in Ultimate Tensile Strength of Weld Nugget of AA6082/ Si_3N_4 Composites with Welding Speed

Figure 20 show the change of UTS with increase of welding Speed, at fixed tool rotation speed of 1950 rpm and fixed tool tilt angle of 2°. UTS of AA6082 decrease from 132 to 130 MPa with increase welding speed from 30 to 50 mm/min. UTS of AA6082/Si_3N_4 /5_P composites decreases from 141 to 123 MPa with increase welding speed from 30 to 50 mm/min. UTS of AA6082/Si_3N_4 /10_P composites decreases from 155 to 147 MPa with increase welding speed from 30 to 50 mm/min. UTS of AA6082/Si_3N_4 /15_P composites decreases from 157 to 150 MPa with increase welding speed from 30 to 50 mm/min.UTS decreases with the increase of welding speed from 30 to 50 mm/min.

Decrease for AA6082/Si_3N_4 /15_P is because of the formation of void defect in the joint, when the welding speed is greater than 50 mm/min. Contradictory effect of welding speed on all the responses was observed as compared to rotational speed. Welding speed affects the quantity of heat that is delivered to the base area of composite plates. Less heat will be dissipation at the weld joint at higher welding speed. Less time is available to disperse heat from composite plates when the tool moves too fast.

3.9 Variation in Ultimate Tensile Strength of Weld Nugget of AA6082/ SiC Composites with Tool Tilt Angle

Figure 21 show the change of UTS with increase of tool tilt angle, at fixed tool rotation speed of 1950 rpm and fixed welding Speed 40 mm/min. UTS of AA6082 decreases from 131 to 130 MPa with increase of tool tilt angle from 1 degree

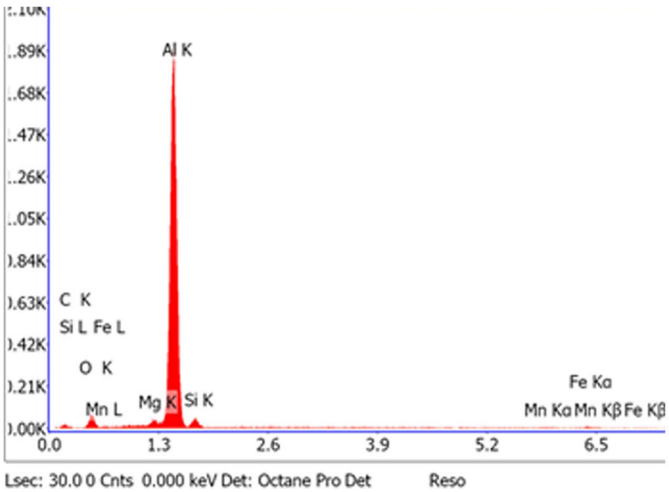

Element	Weight %	Atomic %	Net Int.	Error %
C K	7.78	14.91	3.63	27.81
O K	12.28	17.67	33.63	13.14
MgK	1.2	1.13	18.28	13.54
AlK	73.06	62.35	1142.23	2.82
SiK	3.88	3.18	27.45	13.19
MnK	0.79	0.33	3.5	60.92
FeK	1.02	0.42	3.99	60.2

Fig. 7 EDX pattern of AA6082/ 5% SiC Composite

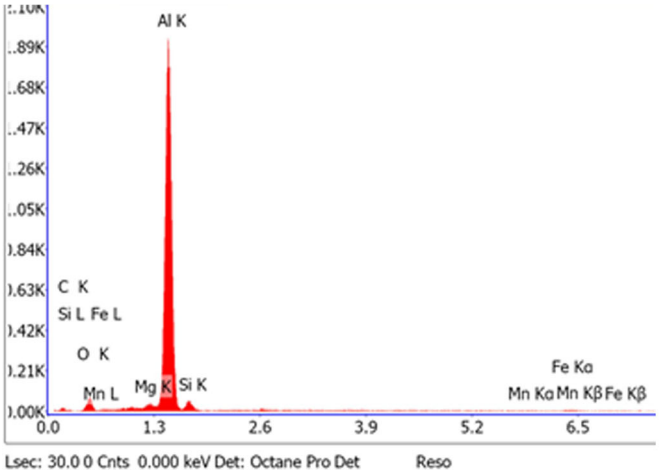

Element	Weight %	Atomic %	Net Int.	Error %
C K	3.12	6.32	1.28	70.68
O K	11.58	17.61	31.22	13.23
MgK	0.89	0.89	13.06	24.2
AlK	77.98	70.28	1166.41	2.65
SiK	4.89	4.23	31.24	12.57
MnK	0.57	0.25	2.35	64.24
FeK	0.98	0.42	3.57	61.11

Fig. 8 EDX pattern of AA6082/10% SiC Composite

to 2 degree. Then it increases from 130 to 132 MPa increase of tool tilt angle from 2 to 3°. Tensile Strength of AA6082/SiC/5_P composite decreases from 119 to 117 MPa with increase of tool tilt angle from 1 to 2°. Then it increases from 117 to 119 MPa increase of tool tilt angle from 2 to 3°. Tensile Strength of AA6082/SiC/10_P composite decreases from 133 to 131 MPa with increase of tool tilt angle from 1 to 2°. Then it increases from 131 to 133 MPa due to increase of tool tilt angle from 2 to 3°. Whereas there is negligible effect of tool tilt angle on tensile strength of AA6082/SiC/15_P composite.

3.10 Variation in Ultimate Tensile Strength of Weld Nugget of AA6082/ Si_3N_4 Composites with Tool Tilt Angle

Figure 22 show the change of UTS with increase of tool tilt angle, at fixed tool rotation speed of 1950 rpm and fixed welding Speed 40 mm/min. UTS of AA6082 decreases from 131 to 128 MPa with increase of tool tilt angle from 1 to 2°. Then it increases from 128 to 132 MPa with increase of tool tilt angle from 2 to 3°. UTS of AA6082/Si_3N_4 /5_P composite decreases from 137 to 130 MPa with increase of tool tilt angle from 1 to 2°. Then it increases from 130 to 134 MPa with increase of tool tilt angle from 2 to 3°. UTS of AA6082/Si_3N_4 /10_P composite decreases from 155 to 145 MPa with increase of tool tilt angle from 1 to 2°. Then it increase from 145 to 152 MPa with increase of tool tilt angle from 2 to 3°. UTS of AA6082/Si_3N_4 /15_P composite decreases from 153 to 150 MPa with increase of tool tilt angle from 1 to 2°. Then it increases from 150 to 155 MPa with increase of tool tilt angle from 2 to 3°. Tensile strength of different specimens is evaluated in order to assess the effect of tilt angle. Results reveal that for all the welding speed, the increase in tool tilt angle initially decreases the tensile strength, reaches a minimum value and then increases. At 2° tilt angle, the heat generation is more, hence tensile strength is less. This shows that the welding speed is inversely proportional to the tensile strength at 2° tilt angle. Higher welding speed at a 2° tilt angle shall be avoided.

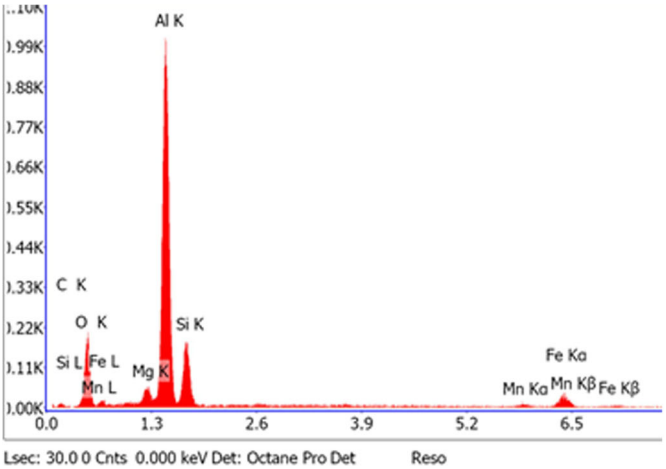

Element	Weight %	Atomic %	Net Int.	Error %
C K	1.2	2.34	0.62	96.15
O K	27.15	39.6	94.1	10.15
MgK	2.22	2.13	25.26	12.44
AlK	48.06	41.57	613.41	4.59
SiK	13.11	10.9	107.41	8.95
MnK	1.24	0.52	5.42	44.26
FeK	7.02	2.94	27.08	13.62

Fig. 9 EDX pattern of AA6082/15% SiC Composite

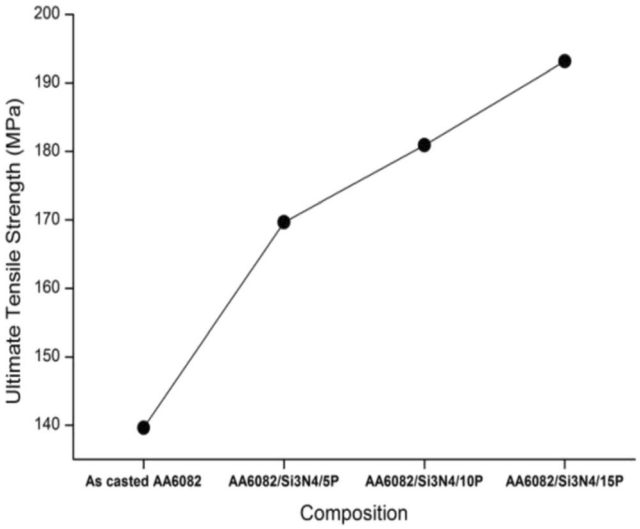

Fig. 10 UTS of AA6082 and AA6082/ Si_3N_4 Composites

4 Discussions

4.1 Microstructure of AA6082/ SiC Composites

Micrographs in Fig. 4 clearly reveal the dispersion of SiC particles in the AA6082 matrix. The distribution of SiC particles is observed to be fairly homogeneous. There are no clusters or agglomeration of SiC particles. Also, there is no segregation of particles along the grain boundaries. There is no separation of SiC particles at the side of grain boundaries in Fig. 5, although there is some clustering of SiC particles. Some particles are located near the grain boundaries due to smaller grain size. But entrapment of particles within grain boundaries is not there. In Fig. 6, SiC particles are uniformly distributed. Hence, the dispersion is considered to be intragranular.

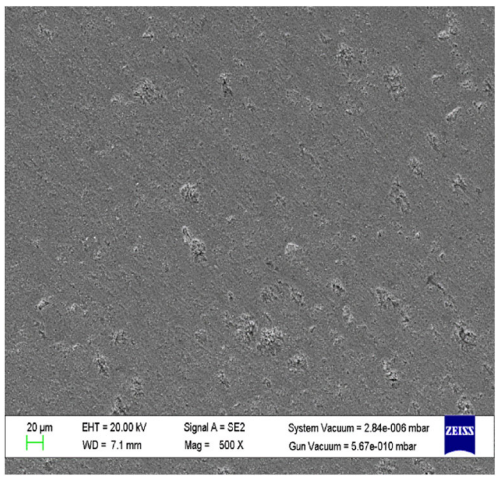

Fig. 11 SEM image of AA6082/ Si_3N_4/5p

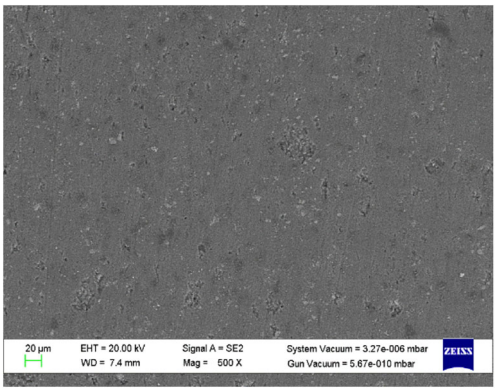

Fig. 12 SEM image of AA6082/ $Si_3N_4/10_P$

4.2 Microstructure of AA6082/ Si_3N_4 Composites

In Fig. 11 SEM images shows proper interface between AA6082 matrix and Si_3N_4 particles. Micrograph in Fig. 12, indicates the presence of Si_3N_4 particles in the AA6082 matrix. The bunching of particles at few places in seen in the microstructure in Fig. 13. a-Al is formed mostly because of thermal mismatch of Si_3N_4 particles and the molten AA6082. Thermal conductivity of Si_3N_4 particles is less in comparison to AA6082 melt. Because of this, the temperature of Si_3N_4 particles will be higher than that of molten AA6082. Therefore, hot Si_3N_4 particles take extra time to cool in solidification process. As a consequence the liquid alloy in the surrounding will be heating up. Nucleation of a-Al in the liquid AA6082 takes place, due to this thermal mismatch.

4.3 Effect of Tool Rotation Speed on the Mechanical Properties of the AA6082 Joints

Two main strengthening mechanisms are grain boundary strengthening and the precipitation hardening. Performance of joint depends on these mechanisms. Microstructure in the various regions, vary with respect to the tool rotation speed. Effect is more prominent is LHDR region. Mechanical properties change

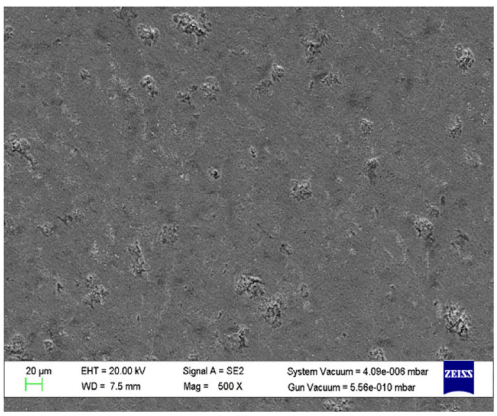

Fig. 13 SEM image of AA6082/ $Si_3N_4/15_P$

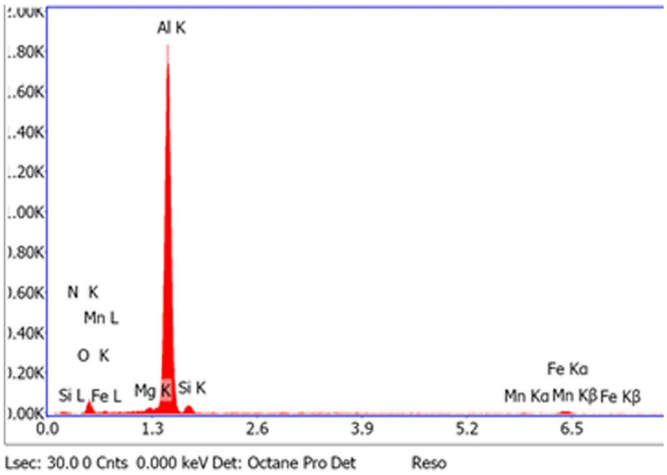

Element	Weight %	Atomic %	Net Int.	Error %
N K	0.29	0.53	0.19	99.99
O K	11.13	17.73	29.75	13.94
MgK	0.67	0.7	9.06	41.36
AlK	79.74	75.29	1108.25	2.85
SiK	4.49	4.07	28.6	13.49
MnK	0.72	0.34	2.85	62.94
FeK	2.95	1.34	10.24	22.85

Fig. 14 EDX pattern of AA6082/5%Si_3N_4 Composite

as per the microstructure. Genvois et al. [16] is of opinion that, Hall–Petch relation can be used to express the amount of grain boundary strengthening. As per Hall–Petch relation the strength or the hardness is inversely proportional to the average grain size of the region. They concluded that fine grains are there in stir zone. Number of grain boundaries are there in fine grains. These grain boundaries resist the motion of dislocations during loading. This is the reason of stir zone displaying higher hardness than the TMAZ. Coarsening of grains took place in the TMAZ. Higher grain size were found mainly in the joints fabricated using higher tool rotation speeds. As per Liu et al. [17], the availability of the grain boundaries is very low. This is because of the coarse grains. Hence obstruction to dislocation motion is less. Which reduces the grain boundary strengthening in the TMAZ. Tensile fracture is observed in the TMAZ region. From this, it can concluded that hardness in the LHDR of the joint affect the tensile strength and elongation. According to Sabari et al. [18], the presence of fine precipitates offers more resistance to the dislocation motion. Therefore it results in high strength or hardness.

During tensile test concentration of load takes place in the softer zone of the joint. This is termed as localization of strain. TMAZ is the softer region. Therefore, the load will be accommodated in the LHDR. Tensile fracture occurred in the LHDR due to concentration of load. Even slight increase in the hardness of LHDR will increase the tensile strength. This is because of resistance to strain localization [19]. Weld joint displays lower elongation than the parent metal. According to Fonda and Deschamps [20], the weakest region alone adds to elongation by strain localization. Although there is reduction in elongation, major change in ductility of AA6082 is not observed due to change in the tool rotation speed.

4.4 Evaluation of Tensile Strength of AA6082/ Si_3N_4 Composites

Increase in UTS of fabricated AA6082/ Si_3N_4 composites with weight percentage of Si_3N_4 particles is shown in Fig. 10. Increase

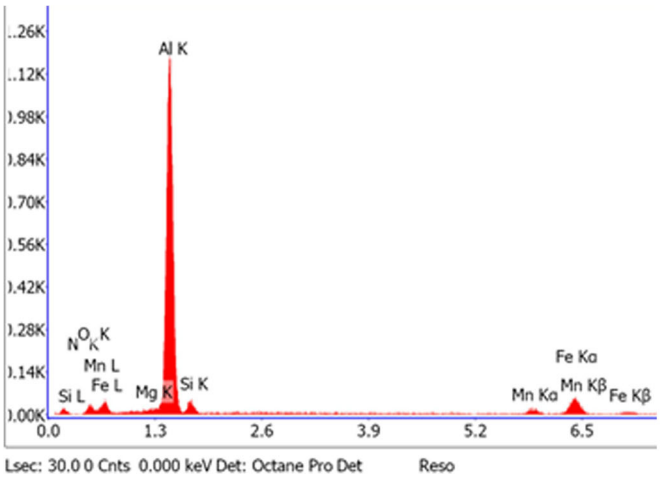

Element	Weight %	Atomic %	Net Int.	Error %
N K	0.13	0.24	0.05	99.99
O K	8.06	13.31	14.08	18.19
MgK	0.29	0.31	2.5	70.09
AlK	79.53	77.82	721.45	3.23
SiK	5.66	5.32	22.15	56.62
MnK	0	0	0	1.49
FeK	6.33	2.99	14.58	56.05

Fig. 15 EDX analysis of AA6082/10 %Si_3N_4 Composite

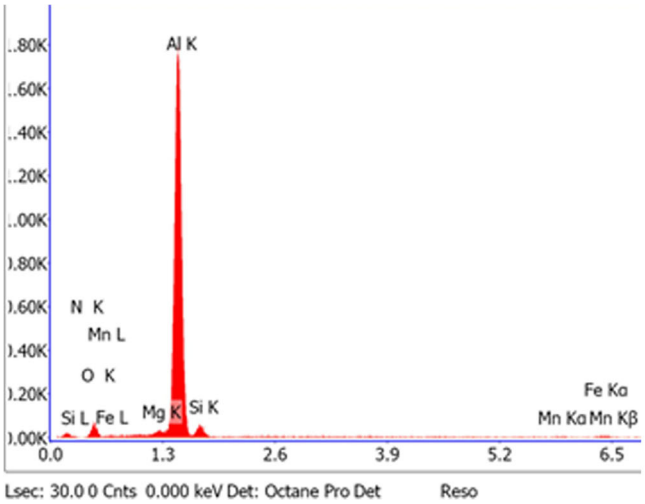

Element	Weight %	Atomic %	Net Int.	Error %
N K	1.57	2.8	1.07	82.94
O K	11.92	18.66	31.58	13.06
MgK	0.91	0.93	12.79	19.1
AlK	77.71	71.72	1113.52	2.79
SiK	5.6	4.96	34.67	12.38
MnK	0.85	0.38	3.41	61.25
FeK	1.44	0.64	5.12	41

Fig. 16 EDX analysis of AA6082/15 %Si_3N_4 Composite

in the tensile strength of AA6082/ Si_3N_4 composites from 140 to 193 MPa is due the addition of hard Si_3N_4 particles in the AA6082 matrix. Hard Si_3N_4 particles transfer their strength to the AA6082 matrix by their strengthening mechanism. This happens because of load transfer from Si_3N_4 particles to AA6082 matrix. Hence, AA6082 matrix provides more resistance to tensile load. Thermal expansion co-efficient of Si_3N_4 particulates is 1.4 to 3.7×10^{-6}/K (https://www.azom.com /properties. Aspx? ArticleID = 53). It is 23.6×10^{-6}/K for aluminium (https://www.amesweb.info/Materials/ Thermal_Expansion_Coefficient_of_Aluminum.aspx). This difference in thermal expansion between the AA6082 and Si_3N_4 particles leads to higher dislocation density in the AA6082 matrix and higher load bearing capacity of hard Si_3N_4 particles. These are responsible for increasing tensile strength of the AA6082/ Si_3N_4 composites. Increases in the amount of low CTE Si_3N_4 particles in the high CTE AA6082 matrix results into the microstructural changes in the matrix. This is the reason of increase in tensile strength of AA6082/Si_3N_4 composites. Further, increase in strength of AA6082/Si_3N_4 composites may be ascribed, to the transfer of load by Si_3N_4 particles to AA6082 matrix. Hence AA6082/Si_3N_4 composites can sustain higher load.

Table 5 show variation in UTS of weld nugget of AA6082/ $Si_3N_4/5_P$, A6082/$Si_3N_4/10_P$ and AA6082/$Si_3N_4/15_P$ composite

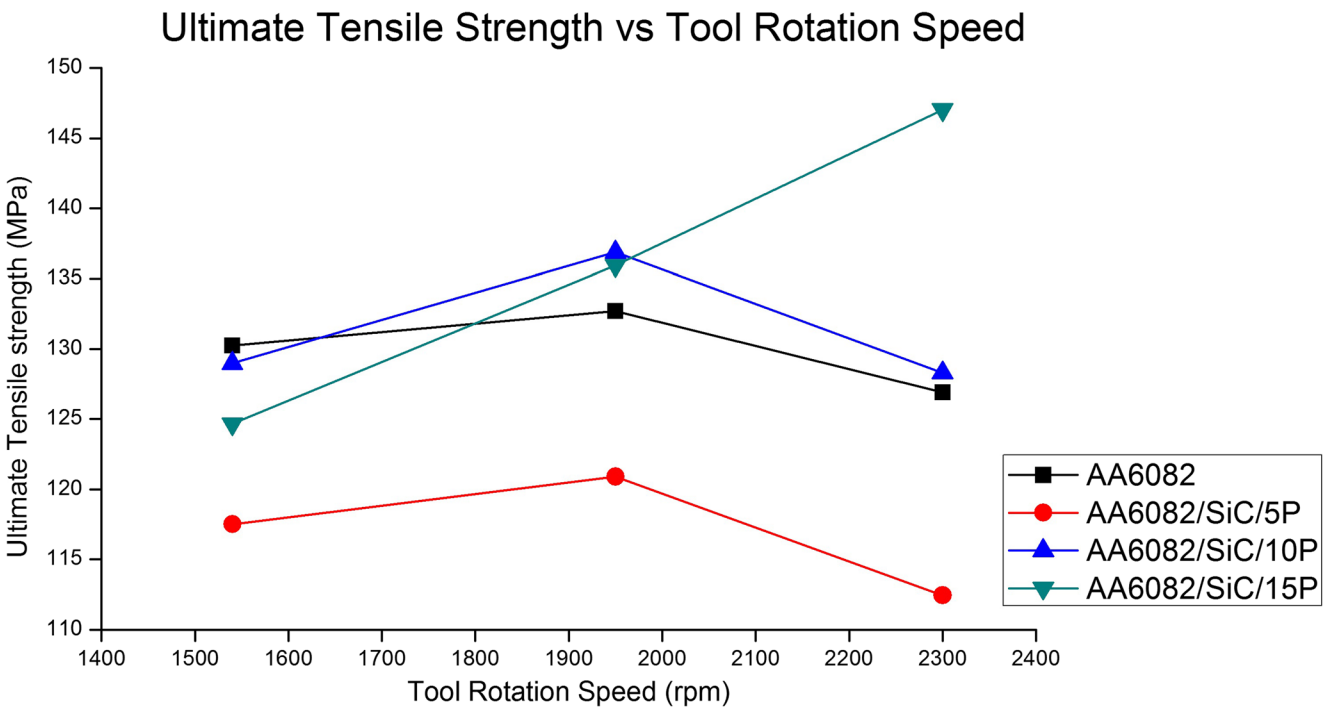

Fig. 17 Change in UTS of AA6082 and AA6082/SiC Composite with Tool Rotation Speed

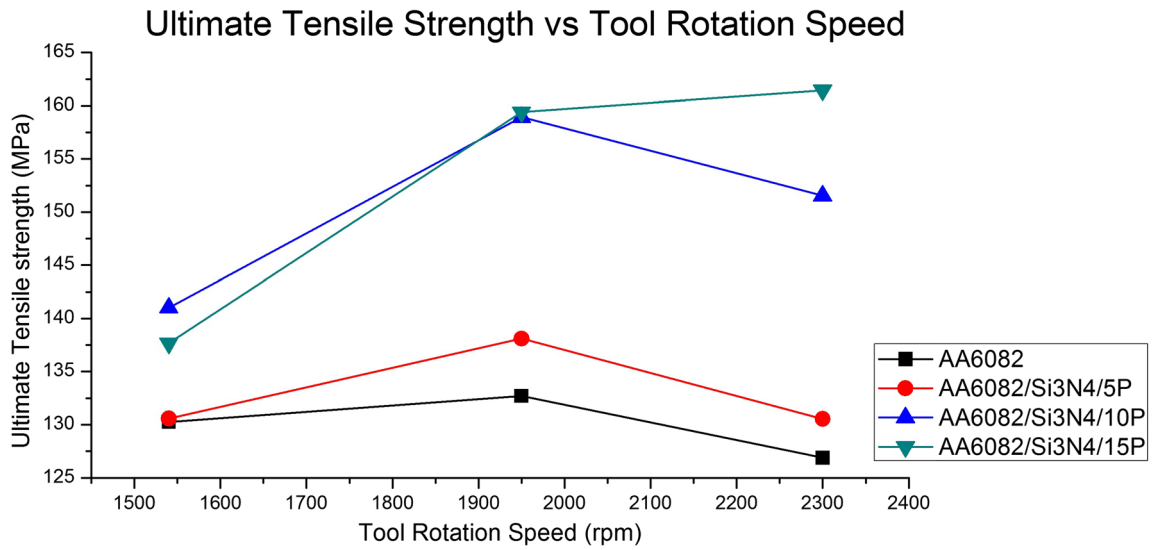

Fig. 18 Variation in UTS of AA6082 and AA6082/ Si_3N_4 Composites with tool rotation speed

during different experiments. Brittle behaviour of the Si_3N_4 particles plays an important role in reducing the ductility of AA6082 matrix. They increase the brittleness in the AA6082/Si_3N_4 composites. Which in turns decrease the amount of ductility in the AA6082/Si_3N_4 composites. Further, increasing the weight percentage of Si_3N_4 particles in the composites resists the flowability of AA6082 matrix. Which decreases the ductility of AA6082 matrix.

4.5 Evaluation of Tensile Strength AA6082/ SiC Composites

Increases in UTS was observed from 140 to 176 MPa with the addition of SiC reinforcements to the AA6082 matrix, as seen in Fig. 2. Modulus increases with increase in volume percent of SiC particles. This is due to strong interfacial bonding between hard SiC particles and AA6082 matrix. Improved adhesion between the solidified AA6082 matrix and the SiC particles is due to the greater metallic character of the reaction layer.

4.6 Effect of Rotational Speed on UTS

Lower tool rotational speed (1540 rpm) produced (a) less heat (b) poor stirring action by the tool pin as rpm are less. Stirring becomes difficult at lower rotational speed as heat input is less. Hence lower tensile strength was obtained. In Figs. 17 and 18, increasing the rotational speed to 1950 rpm increased continuous heat input to the joint. Which created uniform grain refinement. This results in improved tensile strength.

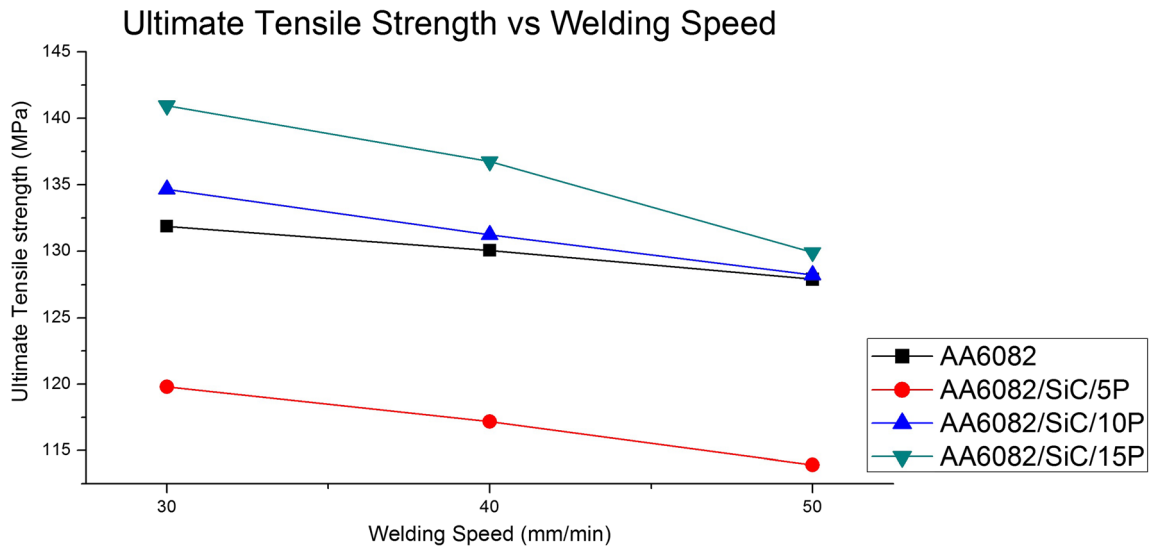

Fig. 19 Variation in Ultimate Tensile Strength of Weld Nugget of AA6082/ SiC Composites with Welding Speed

Among the variables considered in this study, the most influential variable appears to be rotational speed. Rotational speed affects the translation velocity. Very high rotational speeds (>2300 rpm) will increase the strain rate, and create an impact on the FSW process. Greater rotational speed will result in higher temperature. Because of this cooling will be slow in the FSW zone after welding. Higher tool rotational speed produces the extra stirred materials which subsequently moves to the upper surface. This creates cavities in the FSW zone. Therefore FSW shall be carried out at moderate rotational speed. This would result in low heat input and less damage in HAZ.

According to Lee et al. [21], the area of the FSW reduces with decrementing the tool rotation speed. This affect the temperature distribution in the FSW zone. According to Liu et al. [17], as the rotation speed increases, the stirred region extends, and the position of the maximum strain finally moves to the advancing side from the original retreating side of the joint. This shows that the fracture position of the FSW joint is also affected by the rotation speed.

At a particular traverse speed, tensile strength and ductility at lower spindle speed are less. Tensile strength and elongation are enhanced with the increase in rotation speed. Tensile strength acquires maximum value at medium rotational speed. Value falls again at high rotational speeds. As the rotational speed increases, the heat input also increases during FSW. Still, the maximum temperatures are approximately the same in all the rotational speeds. This occurrence can be explained by two reasons; (i) coefficient of friction decreases when local melting occurs, and then decreases with a local heat input; (ii) latent heat absorbs portion of heat input. With the decrease in rotational speed, the temperature reduces within the nugget Zone. To get a FSW region with uniformly distributed fine particles throughout the matrix, the volume fraction of the coarse second phase shall be optimized.

4.7 Effect of Welding Speed on UTS

Figures 19 and 20 show the effect of welding speed on UTS of friction stir welded AA6082/SiC and AA6082/Si_3N_4 composites joints. The UTS of FSW joints was high at the lower welding speed of 30 mm/min. UTS then started decreasing with increase in welding speed. It is observed that higher welding speed decreases the frictional heat input to the AA6082/SiC and AA6082/Si_3N_4 composites. Due to this plastic flow of the AA6082 matrix reduces. Reduced flow causes few cavities in the welded joint. This restricts the grain growth and causes reduction in the breadth of the weld. Hence less tensile strength is obtained.

4.8 Effect of Tool Tilt Angle on UTS

Figures 21 and 22 show the variation in UTS of weld nugget of AA6082/ SiC and AA6082/Si_3N_4 composite with tool tilt angle.Tilt angle affects the vertical and horizontal flow of the weld material. Improper tilt angle creates tunnel and crack-like defects in the welds. At 2° tilt angle, reasons for defects are the insufficient vertical and horizontal flow of the weld material. These defect reduce the strength of FSW joint. Equiaxed grains during FSW are obtained in the nugget zone due to dynamic recrystallization. When the tilt angle is increased more than 2°, there is an increase in average grain diameter. During increase of tilt angle, higher torque and vertical forces are experienced. Increase in both torque and vertical force leads to higher heat input. Result is, higher peak temperature and longer cooling time. Heat exposure time to nugget will also increase. Increasing the tilt angle to 3°, improves the flow characteristics and tensile strength of weld.

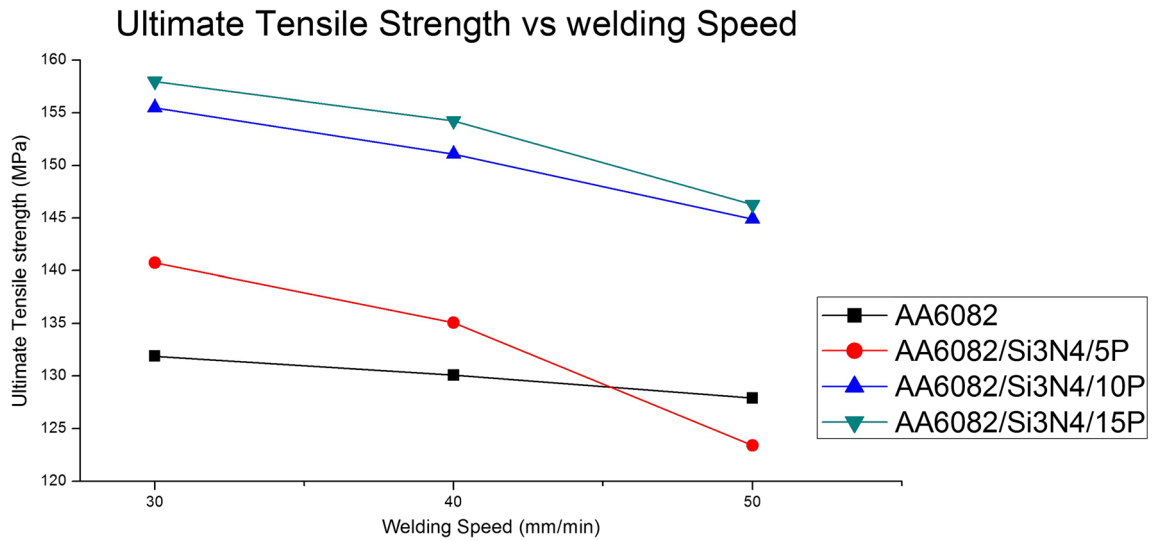

Fig. 20 Variation in UTS of Weld Nugget of AA6082/Si_3N_4 Composites with Welding Speed

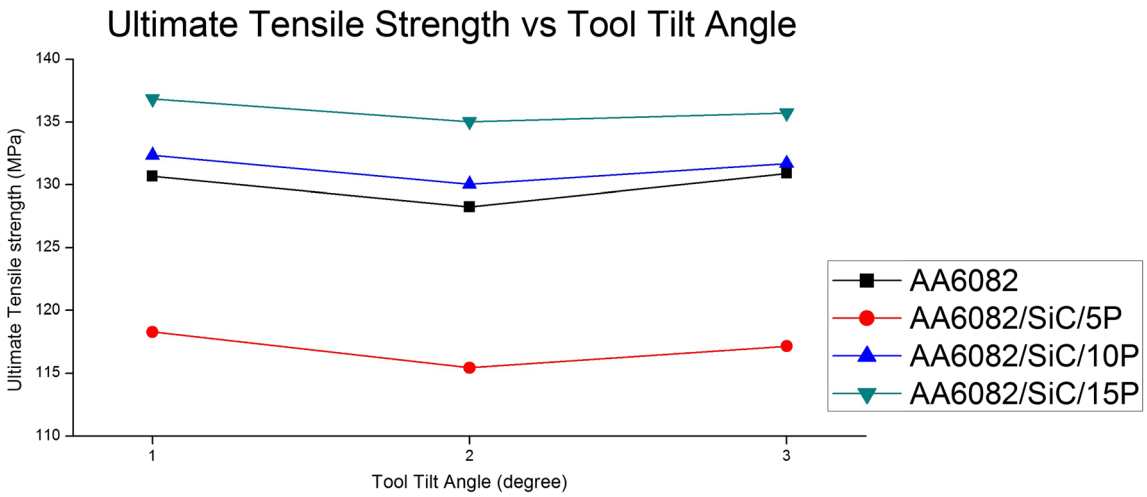

Fig. 21 Variation in Ultimate Tensile Strength of Weld Nugget of AA6082/ SiC Composite with Tool Tilt Angle

4.9 Effect of Tool Rotation Speed on the Joint Quality

Quality of the FSW joint mainly depends on the heat generation and the material flow actions. According to Zhang et al. [22, 23], heat generation and material flow behaviour are classified into three states. These are insufficient state, balance state and excess state. An optimum combination of balance state of heat generation and balance state of material flow yields sound joints.

Tool rotation speed is an important process parameters of the FSW. It affect the amount and rate of heat generation. As a result the material flow is also affected. Heat generation is inadequate at lower tool rotation speed. This is due to poor rubbing of the tool on the plates. But at medium tool rotation speed of 1950 rpm, the FSW joint results in defect free SZ formation. Due to poor heat absorption capability of air, heat is retained in the joint area. Heat accumulates at the FSW joint even at the lower tool rotation speed. Rate of heat generation is not so significant in FSW, because it has a wider preheat zone. Material in the preheat zone is softened during rubbing by tool. On stirring, there is comparatively easy flow of material so the defect free SZ was formed in the FSW joint fabricated at tool rotation speed of 1950 rpm. FSW joint made-up at higher tool rotation speed of 2300 rpm results in formation of defects in the SZ in FSW joints. Due to high rubbing force, excess heat is generated. This results in turbulent flow of materials. The material becomes soft due to the excess plasticization also. This reduces the friction between tool and plate. Reduction in the friction will result in the slipping of material and thereby the defects. This is the reason for defects at higher tool rotation speed of 2300 rpm. Defect free FSW joints are obtained in the tool rotation speeds range of 1500–1950 rpm. This is due to proper balance of heat generation and material flow.

5 Conclusions

In the present work AA6082/Si_3N_4 and AA6082/SiC cast composites with 5, 10 and 15 wt% reinforcement were

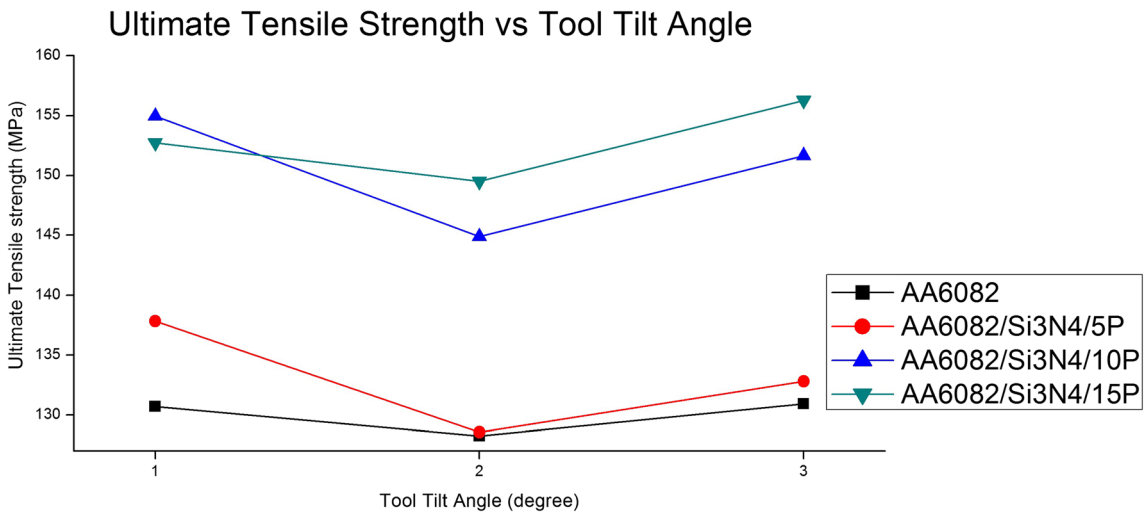

Fig. 22 Variation in UTS of Weld Nugget of AA6082/Si_3N_4 Composites with Tool Tilt Angle

successfully welded by FSW. The welding trials were carried out at different tool rotation speed, welding speed and tool tilt angle by keeping other parameters constant. From mechanical and metallurgical characterization of welded joint, following conclusions are made;

i. Friction stir welding of AA6082/Si_3N_4 and AA6082/SiC cast composites leads to an improvement in the tensile strength due to modification in solidification microstructure of base composite. Homogeneous distribution of SiC particles and strong interfacial bonding between hard SiC particles and AA6082 matrix are dominant reasons for improvement of tensile strength. Hard Si_3N_4 particles transfer their strength to the AA6082 matrix by their strengthening mechanism. This happens because of load transfer from Si_3N_4 particles to AA6082 matrix. Which results in improvement of tensile strength.
ii. Within range of parameters experimented, tensile strength of FSW joint is more sensitive to change in tool rotation speed when compared to welding speed and tool tilt angle. The highest tensile strength of 193 MPa was obtained for AA6082/15 wt% Si_3N_4 composite, at tool rotation speed of 1950 rpm at fixed welding speed of 40 mm/min and fixed tool tilt angle of 2°. Increasing the rotational speed to 1950 rpm, increased continuous heat input to the joint. Which created uniform grain refinement. This results in improved tensile strength.
iii. The optimum parameters to get maximum UTS for AA6082/SiC/5_P and AA6082/SiC/10_P composites are rotation speed (1950 rpm), welding Speed (30 mm/min) and tool tilt angle (3 degree). Maximum UTS for AA6082/SiC/15_P is obtained at 2300 rpm, 30 mm/min and 1 degree.
iv. Optimum parameters to achieve maximum UTS for AA6082/Si_3N_4/10_P and AA6082/Si_3N_4/15_P composites are 1950 rpm, 30 mm/min and 1 degree. Whereas maximum UTS for AA6082/Si_3N_4/5_P is obtained at 2300 rpm, 30 mm/min, and 1 degree.

Data Statement: Experiments have been carried by Author. Data in research paper is of experimental work.

References

1. Murr LE (2010) A Review of FSW Research on Dissimilar Metal and Alloy Systems. J Mater Eng Perform 19:1071–1089
2. Deb RT, Bhadeshiam HKDH (2010) Friction stir welding of dissimilar alloys – a perspective. Sci Technol Weld Join 15:266–270
3. Wert JA (2003) Microstructures of friction stir weld joints between an alu minium-base metal matric composite and a monolithic aluminium alloy. Scr Mater 49:607–612
4. Sharifitabar M, Nami H (2011) Microstructures of dissimilar friction stir welded joints between 2024-T4 aluminum alloy and Al/Mg2Si metal matrix cast composite. Compos Part B Eng 42:2004–2012
5. Xiao BL, Wang D, Bi J, Zhang Z, Ma ZY (2010) Friction Stir Welding of SiCp/Al Composite and 2024 Al Alloy. Sci Forum 638–642:1500–1505
6. Bahrami A, Soltani N, Pech-Canul MI, Gutiérrez CA (2016) Development of metal-matrix composites from industrial/agricultural waste materials and their derivatives. Crit Rev Environ Sci Technol 46:143–208
7. Soltani N, Bahrami A, Pech-Canul MI, González LA (2015) Review on the physicochemical treatments of rice husk for production of advanced materials. Chem Eng J 264):899–935
8. Bahrami A, Pech-Canul MI, Gutierrez CA, Soltani N (2015) Effect of rice-husk ash on properties of laminated and functionally graded Al/SiC composites by one-step pressureless infiltration. J Alloys Compd 644:256–266
9. Bahrami A, Soltani N, Pech-Canul MI, Soltani S, Gonzalez LA, Gutierrez CA, Tapp J, Moller A, Gurlo A (2018) Bilayer graded Al/B4C/rice husk ash composite: Wettability behavior, thermo-mechanical, and electrical properties. J Compos Mater 52(27):1–14
10. Alaneme KK, Idris BA, Olubambi PA (2013) Tolulope, and M. Adewale, Fabrication characteristics and mechanical behaviour of rice husk ash – Alumina reinforced Al-Mg-Si alloy matrix hybrid composites. J Mater Res Technol 2(1):60–67
11. Soltani N, Bahrami A, Pech-Canul MI, González LA, Gurlo A (2018) Surface modification of rice-husk ash (RHA) by Si_3N_4 coating to promote its wetting by Al-Mg-Si alloys. Mater Chem Phys 203:223–234
12. Bahrami A, Pech-Canul MI, Gutiérrez CA, Soltani N (2015) Wetting and reaction characteristics of crystalline and amorphousSiO2derived rice-husk ash and SiO_2/SiC substrates with Al–Si–Mg alloys. Appl Surf Sci 357:1104–1113
13. Rana RS, Rajesh Purohit V, Soni K, Das S (2015) Characterization of Mechanical Properties and Microstructure of Aluminium Alloy-SiC Composites. Mater Today 2:1149–1156
14. Jian H, Ling Z, Huimin L (2015) Effect of tool rotational speed on residual stress, microstructure, and tensile properties of friction stir welded 6061-T6 aluminium alloy thick plate. Int J Adv Manuf Technol 1–9
15. Bilici MK (2012) Application of Taguchi approach to optimize friction stir spot welding parameters of polypropylene. Mater Des 35:113–119
16. Genevois C, Deschamps A, Denquin A, Doisneau B (2004) Quantitative investigation of precipitation and mechanical behaviour for AA2024 friction stir welds. Acta Mater 53(8):2447–2458
17. Liu HJ, Fuji H (2003) Mechanical properties of friction stir welded joints of 1050-H 24 aluminum alloy. Sci Technol Weld Join 8(6):450–454
18. Sree Sabari S, Balasubramanian V, Malarvizhi S (2015) Madusudhan. and G.Reddy, Influence of post weld heat treatment on tensile properties of friction stir welded AA2519-T87 aluminium alloy joints. J Mech Behav Mater 24:195–205
19. Liu HJ, Fujii H, Maeda M, Nogi K (2003) Tensile properties and fracture locations of friction-stir-welded joints of 2017-T351 aluminium alloy. J Mater Process Technol 142:692–696
20. Fonda RW, Bingert JF (2014) Microstructural evolution in the heat-affected zone of afriction stir weld. Metall Mater Trans A 35A: 1487–1489
21. Lee WB, Yeon YM, Jung SB (2004) Mechanical properties related to micro structural variation of 6061 Al alloy joints by friction stir welding. Mater Trans 45(5):1700–1705
22. Zhang XX, Xiao BL, Ma ZY (2011) A transient thermal model for friction stir weld. PartI: the model. Metall Mater Trans A 42:3218–3228
23. Zhang Z, Xiao BL, Wang D, Ma ZY (2011) Effect of alclad layer on material flow and defect formation in friction-stir-welded 2024 aluminium alloy. Metall Mater Trans A 42:1717–1726